Single Bunch Longitudinal Measurements of the Cornell Electron-Positron Storage Ring with the Superconducting RF Cavities*

R. Holtzapple and D. Rice

Laboratory of Nuclear Studies, Cornell University, Ithaca, NY 14853

Abstract

As part of the Phase III luminosity upgrade, the Cornell Electron-Positron Storage Ring (CESR) RF system has been upgraded from normal conducting (NRF) to superconducting (SRF) cavaties. The new superconducting cavities change the overall impedance of CESR and thus change the longitudinal bunch distribution. Measurements of the single bunch longitudinal distribution have been made using a streak camera on CESR with the SRF cavities present. These measurements are compared with earlier measurements on CESR with the NRF cavities. The CESR vacuum chamber impedance is determined from the current dependence of the single bunch charge distribution.

1. Introduction

The Cornell Electron-Positron Storage Ring (CESR) is a 768 m circumference e+e- storage ring operating at a beam energy between 4.7 and 5.6 GeV to study decays of the B meson and the narrow Υ resonances. Between 1997 and 1999, the CESR RF system was upgraded with the installation of superconducting RF cavities (referred to as SRF cavities)[1]. Four single-cell niobium superconducting RF cavities, designed to support 1 ampere of stored current at a peak luminosity of $1.7 \times 10^{33} cm^{-2}s^{-1}$, now provide RF acceleration in CESR. Previously the storage ring relied on four 5-cell normal conducting copper RF accelerating cavities (referred to as NRF cavities). With the NRF cavities, CESR could collide a maximum total current of 350mA and achieve a peak luminosity of $4.5 \times 10^{32} cm^{-2}s^{-1}$. A longitudinal coupled bunch instability, caused by higher-order modes in the NRF cavities, limited higher current collisions and higher luminosity. To overcome the limitations of the 5-cell normal conducting cavities, the single cell superconducting cavities have the advantage of: 1) Operating at higher gradient per cell to reduce the overall number of cells from 20 to 4, 2) having a cell shape that strongly damps higher order modes, 3) a 24cm diameter beam tube that reduces the overall impedance of the cavities. These improvements reduce bunch-to-bunch coupling, thus raising the threshold currents of multibunch instabilities

The longitudinal distributions of charge within the bunches with both NRF and SRF cavities have been measured and compared to determine the change in the overall vacuum chamber impedance in CESR.

* This work was supported by the National Science Foundation.

The measurements with NRF cavities were done using a streak camera borrowed from the Stanford Linear Accelerator Center [2]. The measurements presented here (with SRF cavities) were made with a different unit since acquired by Cornell. For both sets of measurements the camera model is Hamamatsu C1587 with a M1952 high-speed streak unit. We used a streak speed of 1ns/15mm for these measurements. The streak camera and experimental set-up for these measurements are similar to previous measurements [2]. In addition to using a different camera, a periscope has been removed from the streak camera optics and a new diamond turned copper mirror is used as a primary mirror for the SRF cavity measurements.

The measurements presented in this paper were taken with a single bunch of positrons. The measurements were performed when the opportunity for beam time was available. Some of the parameters of CESR are shown in Table 1.

Energy	5.289GeV
Circumference	768.427m
Revolution Period	2.563μsec
RF Frequency	499.765MHz
Horizontal Tune Qx	10.53
Vertical Tune Qy	9.59
Longitudinal Tune Qs	0.053
Harmonic number	1281

Table 1. Parameters of the CESR storage ring.

2. CESR Single Bunch Dynamics

If collective effects are ignored, the standard deviation bunch length in a storage ring can be calculated from the synchrotron radiation integrals from [3]

$$\sigma_\tau = \frac{\alpha}{\Omega_s}\left(\frac{\sigma_\varepsilon}{E_0}\right) = \frac{\alpha}{\Omega_s}\sqrt{C_q E_0^2\left(\frac{I_3}{2I_2 + I_4}\right)} \quad (1)$$

where I_2, I_3 and I_4 are the synchrotron radiation integrals. The term α is the momentum compaction, $\left(\frac{\sigma_\varepsilon}{E_0}\right)$ is the energy spread, Ω_s is the synchrotron tune, E_0 is the nominal energy, and C_q is the constant of $3.84\mathrm{x}10^{-13}$m. The synchrotron integrals and longitudinal parameters that reflect CESR when the streak camera experiments were performed are denoted in table 2.

I_1	8.528m	U_0	1.1434MeV
I_2	$1.047x10^{-1}\,\mathrm{m}^{-1}$	σ_z/E_0	$6.728x10^{-4}$
I_3	$2.300x10^{-3}\,\mathrm{m}^{-2}$	σ_z	$1.719x10^{-2}\,\mathrm{m}$
I_4	$1.482x10^{-3}\,\mathrm{m}^{-1}$	α	$1.11\mathrm{x}10^{-2}$
I_5	$5.092x10^{-4}\,\mathrm{m}^{-1}$	V_{rf}	6.70 MV

Table 2. The synchrotron integral and longitudinal parameters for CESR.

As the intensity of the bunch increases, collective effects that modify the slope of the RF wave have to be included. Collective effects lead to changes in the bunch distribution. Two collective effects examined in the past on CESR are potential well distortion and single bunch coherent instabilities. Past measurements with the NRF cavities present indicate that potential well distortion is the main single bunch longitudinal collective effect in CESR[2]. During these measurements no single bunch coherent instability was registered, up to the highest value of current allowed, with the NRF or SRF cavities.

One of the goals of this paper is to determine the change in the bunch distribution with current (potential well distortion) due to the vacuum chamber impedance, and compare these distributions with the simulated distributions. We use the general formalism of Vlasov's Theory for calculating the distribution of particles in CESR. Under the assumption that the energy distribution remains unchanged, the steady state longitudinal distribution, $\psi(\tau)$, is a function of the resistance (R), capacitance (C), and inductance (L) parts of the vacuum chamber impedance as:

$$\frac{\partial\psi(\tau)}{\partial\tau} = \frac{-eE_0\psi(\tau)}{\sigma_\varepsilon^2\alpha T_0}\left[\frac{V_{rf}\cos(\omega\tau+\varphi) - QR\psi(\tau) + \frac{Q}{C}\int_{-\infty}^{\tau} d\tau'\psi(\tau') - U_0}{1+\frac{eE_0QL\psi(\tau)}{\sigma_\varepsilon^2\alpha T_0}}\right]. \qquad (2)$$

The longitudinal distribution, $\psi(\tau)$, can be determined by numerically by integrating equation 2. These simulated distributions can be fit to the measured bunch distribution to determine the vacuum chamber impedance in CESR.

3. Streak Camera Bunch Distributions

Streak camera profiles of the bunch distribution are 512 pixels in size. Each profile is fit to a function that characterizes the distribution of the bunch. An asymmetric Gaussian function adequately characterizes the bunch shape in CESR and is given by

$$I(z) = I_0 + I_1\exp\left\{-\frac{1}{2}\left(\frac{(z-\bar{z})}{(1+\mathrm{sgn}(z-z)A)\sigma}\right)^2\right\}$$

where I_0=pedestal, I_1=peak of the asymmetric Gaussian. Figure 1 is an example of a CESR bunch distribution profile fit to an asymmetric Gaussian function. The fit determines the mean $\bar{z}$, asymmetry factor A, background level I_0, peak of the asymmetric Gaussian I_1, and width σ of the distribution. The pertinent information retrieved from the asymmetric Gaussian function is the rms width

$$\sigma_z = \text{rms width} = \left\langle \left(z - \langle z \rangle\right)^2 \right\rangle^{1/2} = \left[1 + \left(3 - \frac{8}{\pi}\right) A^2\right]^{1/2} \sigma,$$

the mean of the distribution

$$\langle z \rangle = \text{mean} = \bar{z} + 2\sqrt{\frac{2}{\pi}} A\sigma$$

and the asymmetry factor A. These quantities are the quoted results from the measurements.

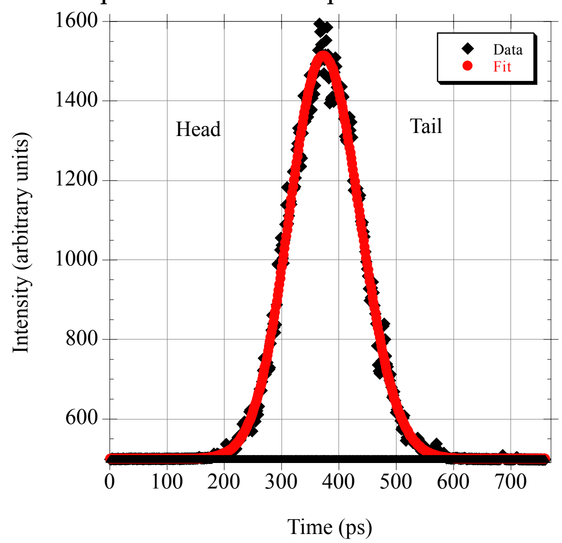

Figure 1 (color). A streak camera profile of the longitudinal distribution of the CESR beam fit to an asymmetric Gaussian function. The head of the bunch (early in time) is to the left. This particular profile was taken with a single bunch current of 9mA.

4. Streak Camera Calibration

The time calibration for the streak camera tube was provided by the Hamamatsu Corporation. Each profile is corrected for time width of each bin (pixel) and this is done by dividing the background subtracted intensity by the calibration curve. The measured, $I_m(K)$ and corrected, $I_c(K)$, image intensity in bin K are related by:

$$I_c(K) = \frac{I_m(K) - I_0}{\text{Calib}(K)}$$

where I_0 is the background determined from the fit to the data. For the streak speed used during these measurements, the calibration curve Calib(K) and corrected time t(K) for each bin is given by:

$$\text{Calib}(K) = 1.2352 + 1.6686\text{x}10^{-3} K - 2.004\text{x}10^{-6} K^2$$

$$t(K) = \int \text{Calib}(K) dK = 1.2352K - 8.343\text{x}10^{-4} K^2 + 6.68\text{x}10^{-7} K^3$$

for pixel K.

5. CESR Single Bunch Longitudinal Dynamics

(i) Single Bunch Low Current Measurements

The low current bunch length is computed from the synchrotron frequency, energy spread, and momentum compaction:

$$\sigma_\tau = \frac{\alpha}{\Omega_s}\left(\frac{\sigma_\varepsilon}{E_0}\right).$$

The momentum compaction and energy spread are determined from CESR's lattice functions. The synchrotron frequency was measured with a spectrum analyzer to be 20.7kHz. This corresponds to a low current bunch length of 57.3ps (17.2mm).

The longitudinal distribution at low current, with minimized collective effects, allows comparisons between the CESR model and the time calibration of the streak camera to be made. The low current positron bunch distribution was measured by taking 10 streak camera pictures with a single bunch present in CESR. A representative single snap shot of the bunch distribution, which has been fit to an asymmetric Gaussian function, is shown in figure 2. The mean bunch length and asymmetry factor extrapolated from the linear fit to the bunch length as a function of current data is shown in table 4.

RMS σ_z	Asymmetry Factor	CESR model σ_z
17.3mm	$3.3\text{x}10^{-4}$	17.2 mm

Table 4. The CESR low current bunch length. The measured bunch length does not have the resolution correction included.

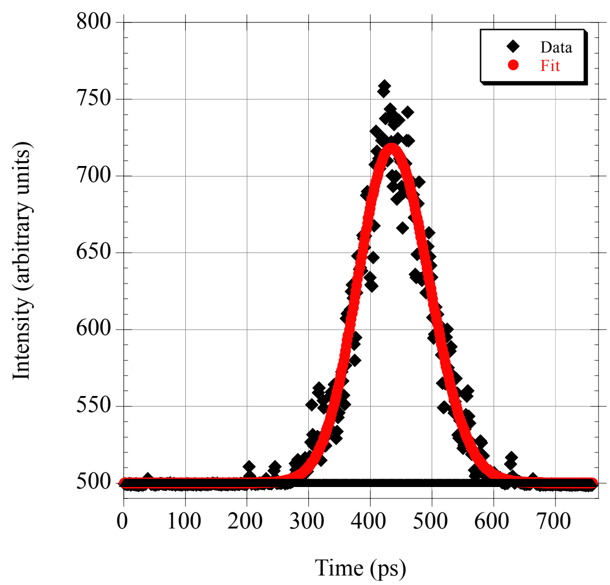

Figure 2 (color). A single picture of the CESR bunch distribution at a current of 0.5mA. The signal to noise at 0.5mA is quite acceptable.

The low current measurements show that the measured bunch length (without resolution correction) is 0.5% larger than the theoretical bunch length. If a resolution correction of 1.73mm(5.77ps) is subtracted in quadrature, the measured and theoretical bunch lengths agree. The resolution of the streak camera is unknown, it depends on many variables. From previous studies of this camera systematic errors, a resolution correction of 1.73mm is within reason [5].

The modifications to the optical path made since the NRF cavity measurements have made a factor of 4 increase in intensity, allowing measurements of the bunch distribution at bunch currents as low as 0.05 mA (0.12 nC).

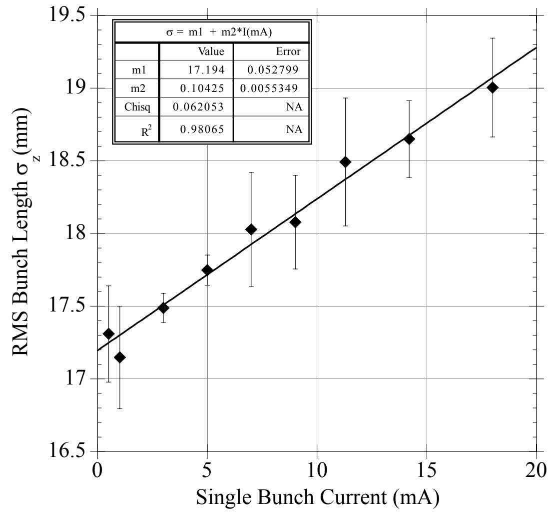

Figure 3. The bunch length in CESR as a function of current.

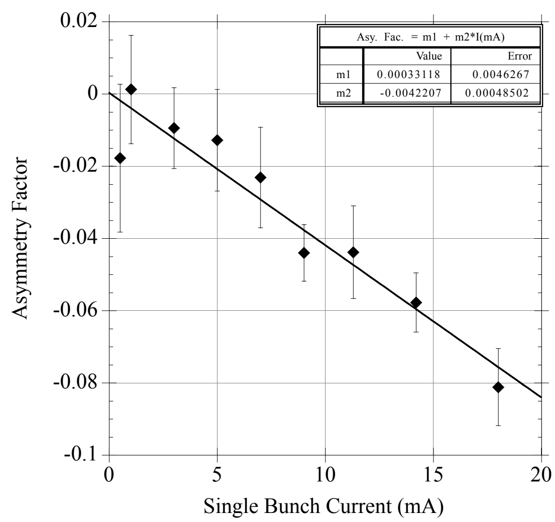

Figure 4. The asymmetry factor as a function of current in CESR. The error bars are r.m.s. spread in values of 10 measurements for each point.

(ii) Bunch length as a Function of Current

The CESR longitudinal bunch distribution between the currents of 0.5 to 18mA was measured with a single bunch present. During these experiments the streak camera slit width was kept at 50μm, as the current increased in CESR, neutral density filters were used to avoid light intensity bunch lengthening. At each current setting, ten streak camera pictures of the bunch distribution were taken. Each picture was fit to an asymmetric Gaussian function and the mean bunch length and asymmetry factor was computed. The mean bunch length and asymmetry factor as a function of current is shown in figures 3 and 4.

There are several noteworthy features of the experimental data:

1) The bunch length increases linearly with current, as denoted by the fit to the data in figure 3. A 0.104mm/mA growth rate in the bunch length is observed over the range of currents measured. A growth rate of 0.065mm/mA was measured with the NRF cavities present [2]. This increase in growth rate can be attributed to an increase in the inductive part of the impedance and/or a decrease in the capacitive part of the impedance.

2) The asymmetry factor also increases linearly as a function of current. A distribution with a negative asymmetry factor has a larger tail than head. With increasing current, the tail of the distribution gets longer, which is a signature of potential well distortion due to the resistive part of the vacuum chamber impedance. These distributions, like the ones displayed in figure 5, can be used to extract the vacuum chamber impedance of CESR. The growth rate of the asymmetry factor with the SRF cavities is -0.0042AF/mA and with the NRF cavities it was -0.0062AF/mA[2] indicating a reduction in the resistive part of the vacuum chamber impedance with the SRF cavities.

3) At each current setting we looked for the presence of synchrotron sidebands around the revolution harmonics. During these experiments no sidebands were observed, hence no coherent longitudinal instability was detected.

(iii) CESR vacuum chamber impedance

We model the CESR vacuum chamber impedance by only its resistive and inductive components (see point 2 below). The vacuum chamber impedance with the NRF cavities present was determined to be $R_{NRF}=1322\pm 310\Omega$ and $L_{NRF}=72\pm 13$nH. One would expect that with the installation of the SRF cavities the overall vacuum chamber impedance has been reduced and the measured bunch distributions should be able to confirm this statement.

Simulated bunch distributions are provided by numerically integrating equation 2. The location of the code is listed in the appendix[6]. Examples of two such the simulated bunch distributions fit to an asymmetric Gaussian function are plotted in figures 6 (a) and (b).

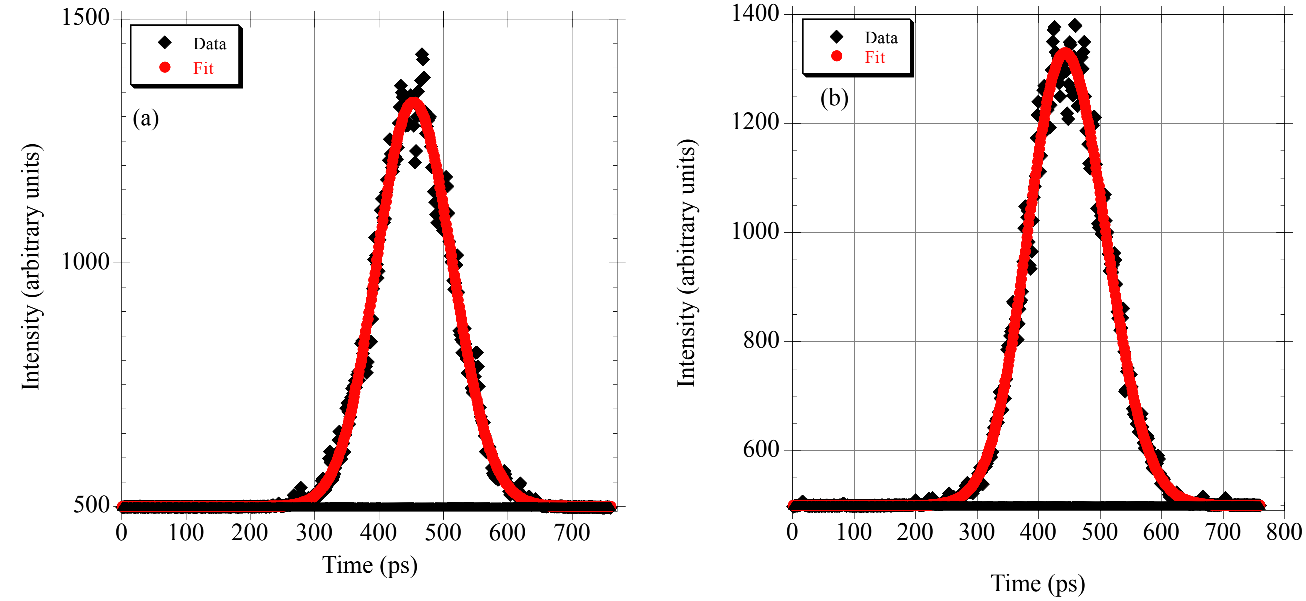

Figure 5 (color). A single streak camera picture of the CESR bunch distribution at a single bunch current of (a) 3mA, and (b) 18mA.

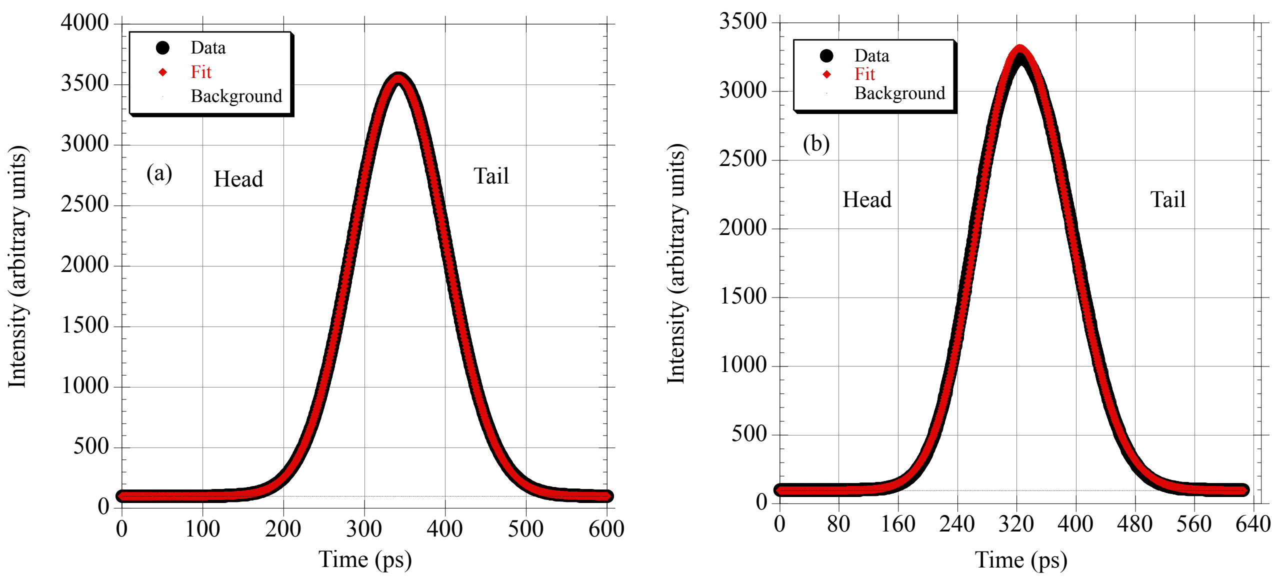

Figure 6 (color). The simulated CESR bunch distribution fit to an asymmetric Gaussian function with: (a) a bunch current of 1mA, and impedance of R=1200Ω and L=90nH. (b) A bunch current of 18mA, and impedance of R=1200Ω and L=90nH.

As with the previous analysis of the vacuum chamber impedance, we assume that the resistance and inductance are constant over the measured range of bunch lengths. The impedance is determined from a χ^2 fit between the simulated and the measured bunch distributions given by

$$\chi^2 = \sum_{i=1}^{n} \frac{\left(S(t_i) - M(t_i)\right)^2}{S(t_i)}$$

where $S(t_i)$ and $M(t_i)$ are the simulated and measured bunch height at time t_i in the distribution. An example of the χ^2 fit is shown in figures 7 (a) and (b).

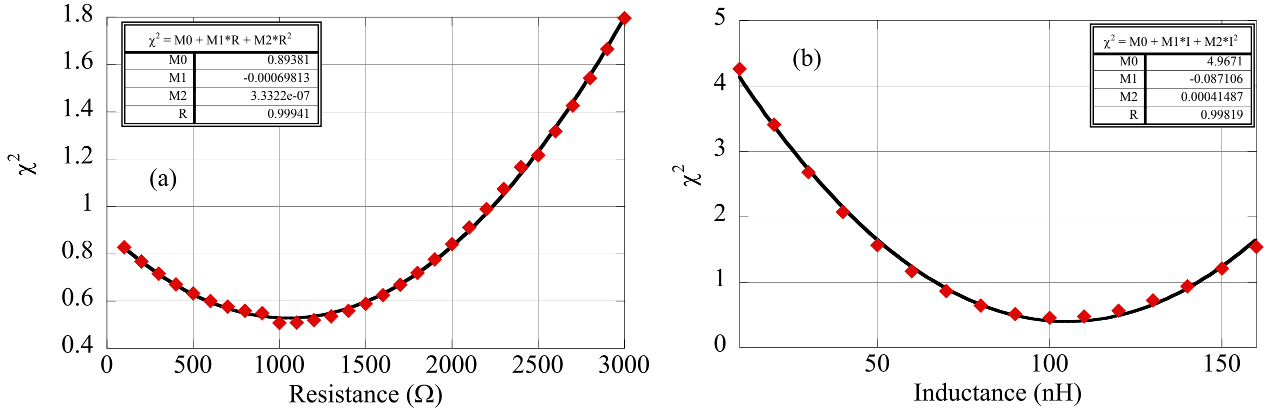

Figure 7 (color). The results from the χ^2 fit for (a) a current of 14mA and inductance of 90nH, (b) a single bunch current of 14mA and resistance of 1100Ω. The resistance and inductance are calculated from fitting the data to a third order polynomial and finding its minimum. In this instance, the resistance in plot (a) is 1048Ω, and the inductance in plot (b) is 105nH.

From the χ^2 fit to the data, the resistance for the CESR ring is R_{SRF}=1016±348Ω and L_{SRF}=96±24nH. The uncertainties are determined by varying the simulation over the range of measurement errors on the asymmetry factor and rms width. Comparisons between the simulated bunch distributions using the above resistance and inductance and the streak camera measurements are shown in figures 8 and 9.

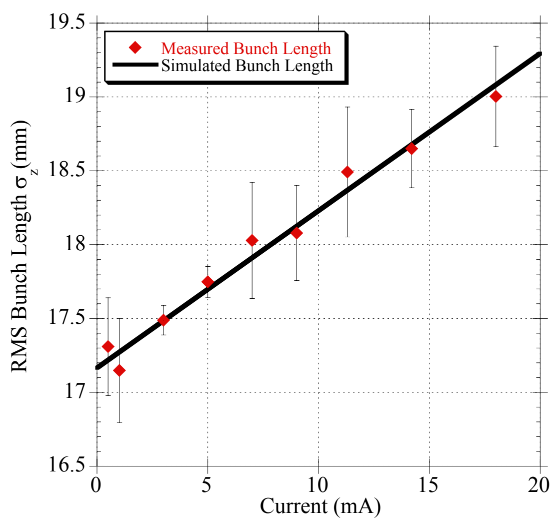

Figure 8 (color). The measured and simulated bunch length as a function of current.

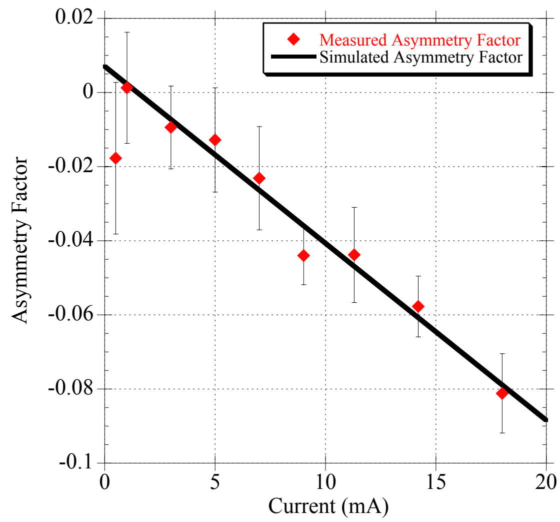

Figure 9 (color). The measured and simulated bunch asymmetry as a function of current.

There are several noteworthy features of the analysis:

(1) The resistive part of the vacuum chamber impedance can also be determined from Higher Order Mode measurements [7]. This measurement gives a resistive impedance of R=939Ω with the SRF cavities present in CESR. This independent measurement confirms our results and claim that the resistive impedance has been reduced with the SRF cavities.

(2) Since both inductive and capacitive parts of the vacuum chamber impedance affect primarily the bunch length (respectively lengthening and shortening) [2], differentiating between an increase in inductance and a decrease in capacitance is quite difficult. The simple model of the vacuum chamber impedance, which ignores the capacitive part, provides a reasonable picture of the measurements. Any capacitive part will likely be exhibited as a change in the inductive part of the impedance. A comparison of the impedance of CESR with the two different cavities shows that the resistive impedance has been reduced and the inductive impedance increased due to the SRF cavities. This increase in the inductive part is overstated in actuality; it is most likely a slight increase in the inductive part and a reduction in the capacitive part of the impedance. After all, the capacitive part of the impedance results from high shunt impedance cavities, such as the NRF cavities, and CESR used to have twenty NRF cavities and now only has four SRF cavities.

(3) Scaling the asymmetry factor and bunch length growth rates can, as a crude method, be used to determine the impedance. Since the resistive impedance is responsible for changing the asymmetry of the bunch distribution, the resistive impedance can be expressed as

$$R_{SRF} = R_{NRF}\left(\frac{AsyGR_{SRF}}{AsyGR_{NRF}}\right) \approx 900\Omega$$

where R_{SRF} and R_{NRF} are the resistive impedance's, and $AsyGR_{SRF}$ and $AsyGR_{NRF}$ are the asymmetry factor growth rates with the SRF and NRF cavities. Since we view the inductive impedance to be responsible for changing the bunch length as a function of current, this inductive impedance can be expressed as

$$L_{SRF} = L_{NRF}\left(\frac{\sigma GR_{SRF}}{\sigma GR_{NRF}}\right) \approx 115\text{nH}$$

where L_{SRF} and L_{NRF} are the effective inductive impedance's, and σGR_{SRF} and σGR_{NRF} are the bunch length growth rates with the SRF and NRF cavities present. The scaling method provides a result for the impedance that is quite reasonable compared to other more complicated ways of extracting the impedance.

6. Conclusions

Measurements of the bunch distribution in CESR show that potential well distortion leads to some asymmetry and lengthening of the beam distribution at high current and that no single bunch coherent instability was apparent. From the measured bunch distributions, we were able to determine vacuum chamber impedance, by modeling it as a sum of the inductive and resistive parts. By comparing the measured bunch length dependence on the current with simulations, the vacuum chamber impedance was determined to have a resistance of $1016 \pm 348\Omega$ and an inductance of 96 ± 24nH.

The low current single beam bunch length measurements confirmed our understanding of the streak camera and validated our theoretical model of CESR. Comparing previous bunch distribution measurements with the NRF cavities in CESR, the new SRF cavities have reduced the resistive part and increased the capacitive part of the CESR impedance. This change in impedance, as well as increased damping of higher order modes, has reduced the threshold of the longitudinal dipole-mode coupled bunch longitudinal instability, which, along with longitudinal feedback, has allowed higher current and higher luminosity running for CESR.

7. Appendix Beam: Numerical Integrating Software

The numerical integrating software, called LNCSB.F77, is contained in the [cesr.mslog.impedance.calc] directory. The LNCSB.F77 instruction manual is located at http://cesrelog.lns.cornell.edu/mslog/impedance/calc/lncsb.html. The input beam parameters used for the simulation are listed in table 2. The software was written by Mike Billing and Matthew Stedinger[6].

8. Acknowledgments

The authors would like to thank John Barley, William Lucas, and Robert Meller for building a fast trigger for the streak camera, and Don Hartill for providing the diamond turned copper mirror.

9. References

[1] Belomestnykh, S., et al., “Superconducting RF System for the CESR Luminosity Upgrade: Design, Status, Plans”. SRF 960529-02.

[2] Holtzapple, R.L., et al., "Single Bunch Longitudinal Measurements at the Cornell Electron-Positron Storage Ring", Phys. Rev. ST Accel Beams 3, 034401, 2000.

[3] Helm, R. H., et al., "Evaluation of Synchrotron Radiation Integrals", SLAC, SLAC-PUB-1193, March 1973. 2pp. Presented at Particle Accelerator Conf., San Francisco, Calif., Mar 5-7, l973. Published in IEEE Trans.Nucl.Sci.20:900-901,1973 (issue No.3)

[4] Haissinski, J., "Exact Longitudinal Equilibrium Distribution of Stored Electrons in the Presence of Self-Fields," Il Nuovo Cimento, Vol. 18B, N.1, 11 November 1973, p. 72.

Billing, M., ”Bunch Lengthening via Vlasov Theory”, CBN 80-2, 1980, 15pp. The updated software was written by M. Stedinger and M. Billing[1998].

Chao, A.W., "Physics of Collective Beam Instabilities in High-Energy Accelerators", New York, USA:Wiley (1993) 371p.

[5] Holtzapple, R.L., “Experimental Techniques for the CESR Streak Camera”, CBN 01-2, 9pp.

[6] Billing, M.,”Bunch Lengthening via Vlasov Theory”, CBN 80-2, 1980, 15pp. The updated software was written by M. Stedinger and M. Billing[1998].

[7] Billing, M., Private Communication.